Cable Force Determination Using Phase-based Video Motion Magnification and Digital Image Correlation

[1]Wenbing Chen, [*2]Banfu Yan, [3]Jingbo Liao, [4]Lei Luo, [5]You Dong

[1]Ph.D Candidate, College of Civil Engineering, Hunan University, Yuelushan, Changsha, Hunan 410082, P.R. China; E-mail: cwb1993@hnu.edu.cn

[2]Associate Professor, College of Civil Engineering, Hunan University, Yuelushan, Changsha, Hunan 410082, P.R. China; Key Laboratory for Wind and Bridge Engineering of Hunan Province, Changsha 410082, Hunan, China; E-mail: yanbanfu@hnu.edu.cn

[3]Senior Engineer, State Key Laboratory of Bridge Engineering Structural Dynamics, Chongqing Engineering Research Center for Intelligent Monitoring of Bridge and Structures, China Merchants Chongqing Communications Research & Design Institute, Chongqing 400067, China; E-mail: liaojingbo@cmhk.com

[4]Ph.D Candidate, College of Civil Engineering, Hunan University, Yuelushan, Changsha, Hunan 410082, P.R. China; E-mail: ll_1926@163.com

[5] Assistant Professor, Department of Civil and Environmental Engineering, The HONG KONG Polytechnic University, Hong hum, HONG KONG, China; E-mail: you.dong@polyu.edu.hk

*Corresponding author: Banfu Yan

Mobile： +86-13973171772

E-mail address: yanbanfu@hnu.edu.cn

Abstract

The mode shape-aided method provides a simple and effective way for cable force determination, which, however, requires accurate parameter identification of the cable structure. This paper proposes a phase-based video motion magnification to process the image sequences of a cable. Digital image correlations were engaged to measure the dynamic displacement-time history, through tracking the surface characteristic features of the cable. Thereafter, a frequency-domain decomposition technique was applied to extract the natural frequency and mode shape of the cable from the displacement-time history measurements. The identified cable mode shapes, along with a tensioned pinned-pinned cable model, were used to estimate the cable force. The accuracy of the proposed methodology was subsequently verified through laboratory testing on an inclined cable model and field-testing on a typical hanger cable of a real-world arch bridge, respectively. Overall, the study results indicated that the proposed methodology could expediently and cost-effectively estimate the tension forces of a cable with reasonably acceptable identification accuracy.

Keywords: Cable force; Mode shape; Video motion magnification; Digital image correlation

1. Introduction

Vibration-based methods for cable force determination have been widely investigated for application to in-service bridges, due, in part, to their simplicity and cost-effectiveness [1,2]. For the ease of practical engineering applications, numerous classical methods such as empirical explicit expressions, approximate formulations, and iterative solutions have been proposed to determine the effective length of cables with pure pinned or clamped end conditions including their sag effects and flexural rigidity [3-5]. Note that for the existing in-service cable-stayed bridges, the installations of multiple intermediate dampers introduce the difficulties of constructing a solvable frequency equation in a conventional manner to identify the complex relationship between the measured natural frequencies and cable forces.

To avoid the difficulties resulting from the multiple intermediate support-induced complex boundary conditions, Yan et al. [6,7] proposed a mode shape-aided method to estimate the cable force independent of the complex boundary conditions. The core idea of the approach is to transform the cable-force estimation problem from the classic procedures of formulating and solving the equations of motion of the cables with complex boundary conditions to a simpler problem of identifying the mode shape of the original cable and thereafter, finding its modal nodes with zero transverse displacements. An equivalent segmental model with the effective length of any two zero-amplitude points can always be determined in the form of a tensioned beam with pinned-pinned end conditions. Chen et al.[8] have successfully employed a similar concept of combining the mode shape functions with the measured natural frequencies to determine the effective length of a cable with complex boundary conditions. With this concept, the cable force is quantitatively determined using an explicit formulation similar to that for the case of cables with hinged boundary constraints.

The mode shape-based approach appears to be attractive due to its simplicity, convenience, and acceptable identification accuracy. However, in practical engineering applications, the accurate identification of the mode shape of the cable is not an easy task. For the classical accelerometer or velocimeter-based modal identification, using output-only techniques such as frequency-domain decomposition (FDD) and stochastic subspace identification (SSI), the identification accuracy is a function of the quality, position, and density of the accelerometers or velocimeters [9,10]. The dense installation of the wired or wireless accelerometer or velocimeter for stayed cables or hanger cables is obviously a laborious and time-consuming work since it is generally difficult to access the top segment of the cable via construction machinery even under traffic interruption.

Digital image correlation (DIC)-based vision system is one of the most popular non-contact displacement and strain measurement techniques. The advantages associated with the DIC technique include high accuracy at the sub-pixel level, long-distance multi-point non-contact test, simple equipment, and easy implementation.[11] At present, the integer-pixel registration algorithms for fast normalized cross-correlation and Fourier transform cross correlation (FTCC) as well as the more efficient sub-pixel registration algorithm for inverse-compositional Gauss–Newton (IC-GN) have been considered as standard solutions for accurate identification of displacements in the DIC method.[12] It is also worth noting that various researchers[13,14] have used the DIC method successfully for bridge deflection measurement. Once the DIC technique has been executed, the conventional modal identification methods in the time or frequency domain can then be employed to extract the modal parameters from the displacement-time histories of the multiple marked targets or marker-less region of interests (ROIs) over the cable structure. The accuracy of the DIC-based modal identification relies deeply on the quality of the surface characteristic features of the ROIs as well

as the tracking error of some ROIs with no apparent pixel-level displacement. Otherwise, any contrasting features may result in the degradation of the identified modal shape.

Recently, the Freeman Team at the Massachusetts Institute of Technology (MIT) developed an innovative computer vision technique, termed as video motion magnification, to enhance the invisible signals of the naked eye.[15-17] The motion magnification employs the following modulations: a time-frequency band pass filter, amplification to the modal motion of interest in a specific frequency band, and final video reconstruction to amplify the small motions in videos. The adopted motion magnification algorithms include the Eulerian motion magnification based on Laplacian pyramid decomposition,[15] phase-based motion magnification (PMM) via complex-valued steerable pyramids,[16] fast phase-based motion magnification (FPMM) via Riesz pyramids[17] and other improved algorithms such as phase-based motion magnification using the Hermite transform,[18] efficient motion magnification system,[19] and multi-scale adaptive factors video acceleration magnification method.[20] Among these algorithms, the PMM is the most popular since this method can significantly reduce the noise in the reconstructed videos via a noise shifting mechanism and support a larger video magnification rate. However, its efficiency is strictly dependent on the number of pyramid decomposition layers, which often requires a heavy memory space and is indeed, a time-consuming task. The FPMM has the advantage of real-time video processing. However, its performance is slightly worse than PMM.

Structural dynamical applications of PMM have been reported in modal frequency identification and mode shape extraction studies. Chen et al.[21,22] and Yang et al.[23] conducted laboratory experiments to validate the PMM in magnifying the motion video for a given mode of interest and successfully employed the canny edge detection method to estimate the operational

deflection mode shape of the experimental model. Chen et al.[24] and Shang et al.[25] also successfully extended the PMM algorithm to in-situ measurement of displacements and operational mode shape of real structures. Sarrafi et al,[26] on the other hand, employed the phase-based motion estimation and phase-based motion magnification techniques to estimate the structural motion and operational deflection mode shapes of wind turbine blades from an array of captured image sequences including damage detection. Molina-Viedma et al.[27] proposed an approach integrating DIC and PMM to explore the characteristics of the DIC mode shapes at high frequencies when the amplitude of the displacements is significantly increased. As stated by Yang et al.,[23] the PMM has two special characteristics, namely: (a) providing high-resolution mode shapes when there is no obvious contrasting surface characteristic feature on the structure, and, (b) capability to resolve closely-spaced modes. Note that for a typical cable with pinned or clamped end conditions, its modal frequencies are approximately multiples of the fundamental frequency, which indicates that the PMM is adaptable to identify the dynamical characteristics of the cable with no closely-spaced modes.

In this study, an effective non-contact target-free vision system integrating the mode shape with a combination of innovative PMM and DIC techniques was proposed for cable force determination. The proposed approach not only avoids the difficulty of establishing and solving the frequency equation of complex cable structures, but it also transforms a complex identification problem to a mode shape identification based on PMM and DIC techniques from the video image sequence. The paper is organized as follows: we first introduce the non-contact target-free vision system in the framework of PMM for mode shape-aided cable force determination. Next, a laboratory experimentation test on tension force determination of an inclined cable using a PMM-

based vision system is presented to demonstrate the effectiveness of the proposed methodology. Thereafter, a practical field test on hanger cables of a real through-type arch bridge is performed to estimate their tension forces. And lastly, a summary of the key findings, conclusions, and recommendations drawn from the study is presented.

2. Study Methodology

2.1. *Work plan and flowchart*

As shown in the flowchart in Fig. 1, the mode shape-aided cable force determination based on the PMM and DIC techniques consists of four primary steps, namely:

- Step (a): In this step, experiments were performed using a digital video camera (Panasonic Lumia GH5 with a Panasonic lens with a focal length of 100~400 mm) to capture the image sequences of a candidate hanger cable of an arch bridge.
- Step (b): During this step, the PMM was employed to amplify the interested modal motion in a specific frequency band of the cable. The PMM operations included general video decomposition, temporal filtering, phase denoising, and the final video reconstruction process.
- Step (c): The operational deflection mode shape was extracted from the motion-magnified video corresponding to a certain resonance frequency via DIC technique in this step.
- Step (d): In this step, the mode shape-aided approach proposed by Yan et. al.[6,7] is then employed to estimate the tension force of the cable with unknown boundary conditions.

For the third-order mode and higher, at least two modal nodes with zero displacements usually exits. The segmental length at any two modal nodes can be considered as the effective length of a

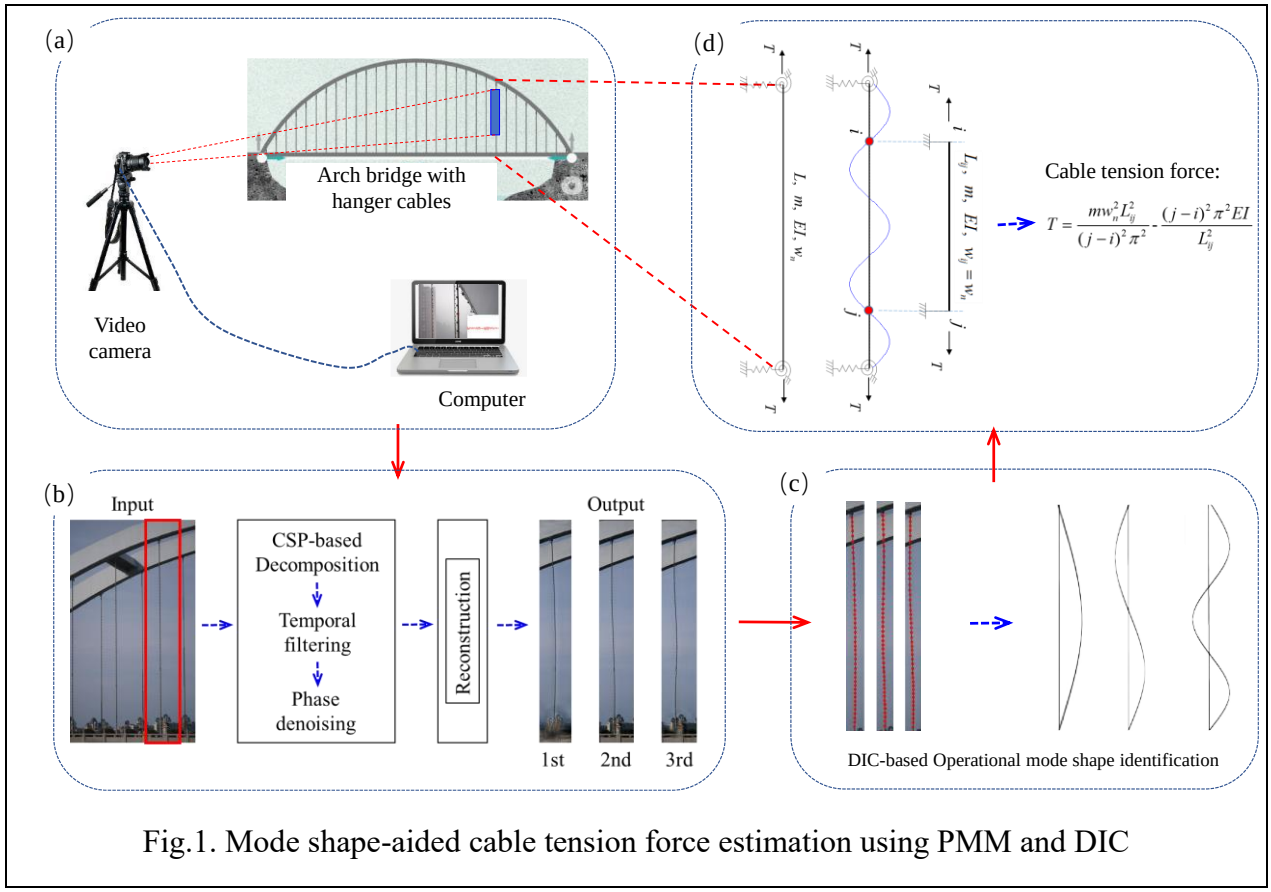

Fig.1. Mode shape-aided cable tension force estimation using PMM and DIC

pinned-pinned cable, from which the cable force can be easily determined based on the traditional formulation for a pinned-pinned tensile beam model. In addition, the approach integrating both the DIC-based target tracking and FDD-based output-only modal identification techniques was used to extract the modal parameters of the cable under slightly higher excitations for comparisons with those using the above-proposed methodology.

2.2. *Phase-based motion magnification (PMM)*

PMM can amplify the motion in the frequency bands of interest by magnifying the phase variations and the band-pass temporal filtering of the video. Fig. 2 shows the principle of the PMM based on the core algorithm of a complex-valued steerable pyramid (CSP). The process is categorized into four steps as follows:

Step (a): In this step, the input video color images are converted from general RGB color space to YIQ color space, and the Y component with luminance information is used for further processing.

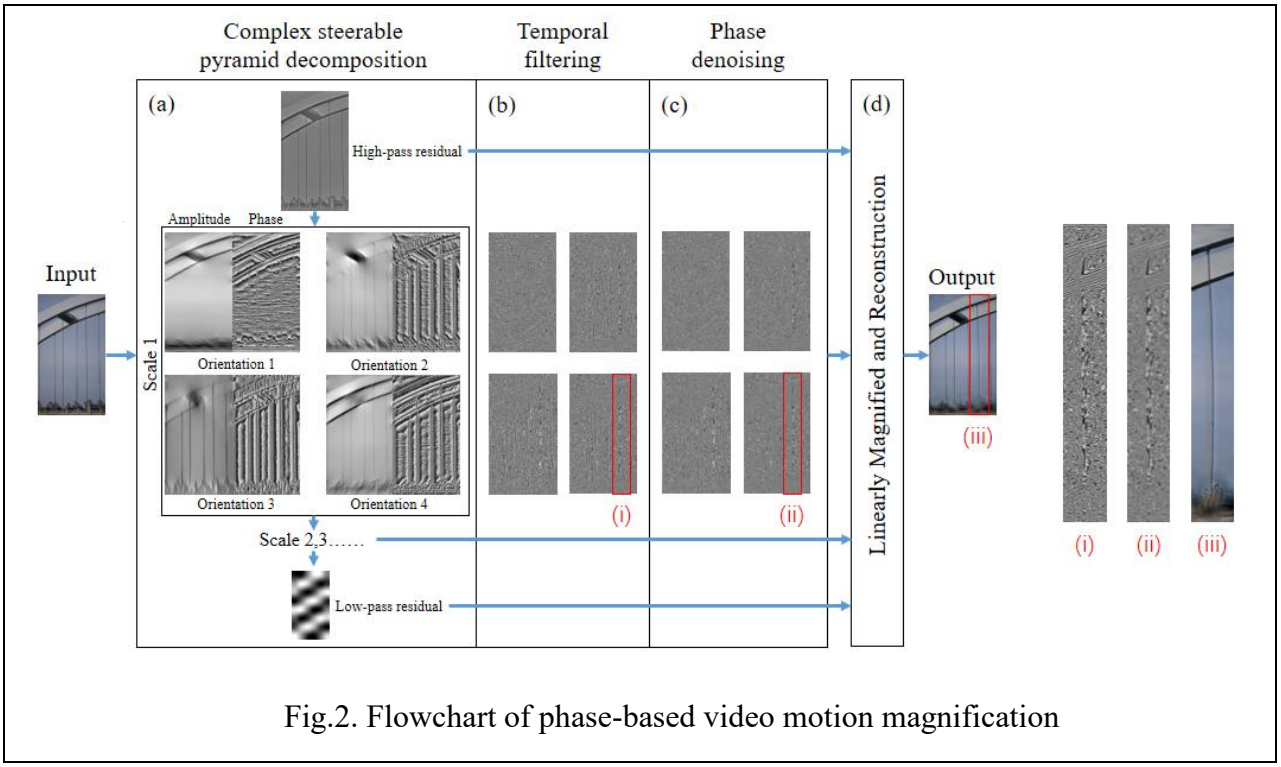

Fig.2. Flowchart of phase-based video motion magnification

The 2D FFT is employed to convert each video image from spatial domain to frequency domain for the next CSP processing, which decomposes the center-symmetric frequency-domain image into frequency-domain sub-bands in the forms of octave, half-octave, and quarter-octave in the tangential and radial directions. Taking octave as an example, the image in the frequency-domain is evenly divided into four times in the tangential direction to generate a total of eight data sets (axisymmetric). Each data set is then divided into half of the original in each radial direction. The termination condition is generally defined as $\log_2(0.5W_{\min}) < 10$ Pixel, where $W_{\min}$ is the length of the image's short side. Each sub-band image in the frequency-domain is transformed to the spatial domain via 2D inverse FFT. The local phase and amplitude over time at every spatial scale and orientation of a steerable pyramid are then calculated as shown in Figure 2.a, where only the phase and amplitude maps at the level of scale 1 and the four outmost radial orientations, namely high-pass residual and low-pass residual images, are plotted).

Step (b): In the second step of the PMM process, the phases at each location, orientation, and

scale are then independently band-pass filtered in the temporal domain.

Step (c): The band-pass filtered phases corresponding to the motion are generally denoised using the amplitude-weighted spatial smoothing technique to increase the quality of the phases.

Step (d). Finally, each temporally filtered phase is linearly magnified by an amplification factor, and the video is reconstructed to attain the motion magnification results. Note that the magnified gray scale images in the Y-channel with the restored IQ-channels are restored to the original RGB color space in this step.

A C++ version of the CSP program employing an 8-orientations quarter-octave CSP and finite impulse response (FIR) temporal filter was built for phase amplification. In practical applications, as the PMM is employed to extract the amplified motion corresponding to a certain resonance frequency of the cable, prior knowledge of the vibration frequencies of the cable should be provided as the central frequency or reference datum of a specific frequency band. In this study, as the image sequences of the cable were recorded, the DIC, integrating integer-pixel image registration algorithm FTCC with subpixel registration algorithm IC-GN, was employed to extract the displacement-time history of a selected point of interest on the cable with distinct surface characteristic features.

The FFT of the displacement-time history is then implemented to attain its frequency spectrum, from which the natural frequencies of the cable can be extracted via the traditional peak picking approach. In the study, it was noted that the modal frequencies of the cable are approximately multiples of the fundamental frequency without closely spaced modes. Hence, it is easy to correctly identify the mode order and the corresponding resonance frequency. The natural frequencies are thus considered as the central frequency of specified band-pass filtering for phase variations in the

PMM procedure. Lastly, the amplified motion of the cable corresponding to a certain resonance frequency is obtained.

2.3. *DIC-based operational deflection mode identification*

As the image sequences of the motion-magnified video via PMM are captured, the next step is to extract operational deflection modes from the motion-magnified video corresponding to the resonance frequency of the cable. As shown in Fig. 3, rather than the common Cannon edge detection method, DIC is again employed to extract the operational deflection shapes of the cable. The implementation process is categorized into four steps, namely:

Step (a): For a motion-magnified video corresponding to a certain resonance frequency of the cable, multiple target points (red) along the cable are first virtually marked at the first frame of the image sequence as their original positions.

Step (b): DIC is used to track the motion of the target points along the cable. The displacement-time history of a target point with a relatively larger amplitude is estimated. Thereafter, a peak picking is performed to locate the time instants T_1, T_2,…, T_k,… and T_n with positive (or negative) displacement peak in each cycle.

Step (c): The displacements of all the target points at time instant T_k $(k = 1, 2, ..., k, ...n)$ can be displayed in the form of a snap shot and denoted as the instant operational deflection shape of the cable.

Step (d): The addition of n groups of instant operational deflection shapes is then normalized and fitted to a Sine-type mode shape, from which the mode nodes of the cable at each mode can be easily identified.

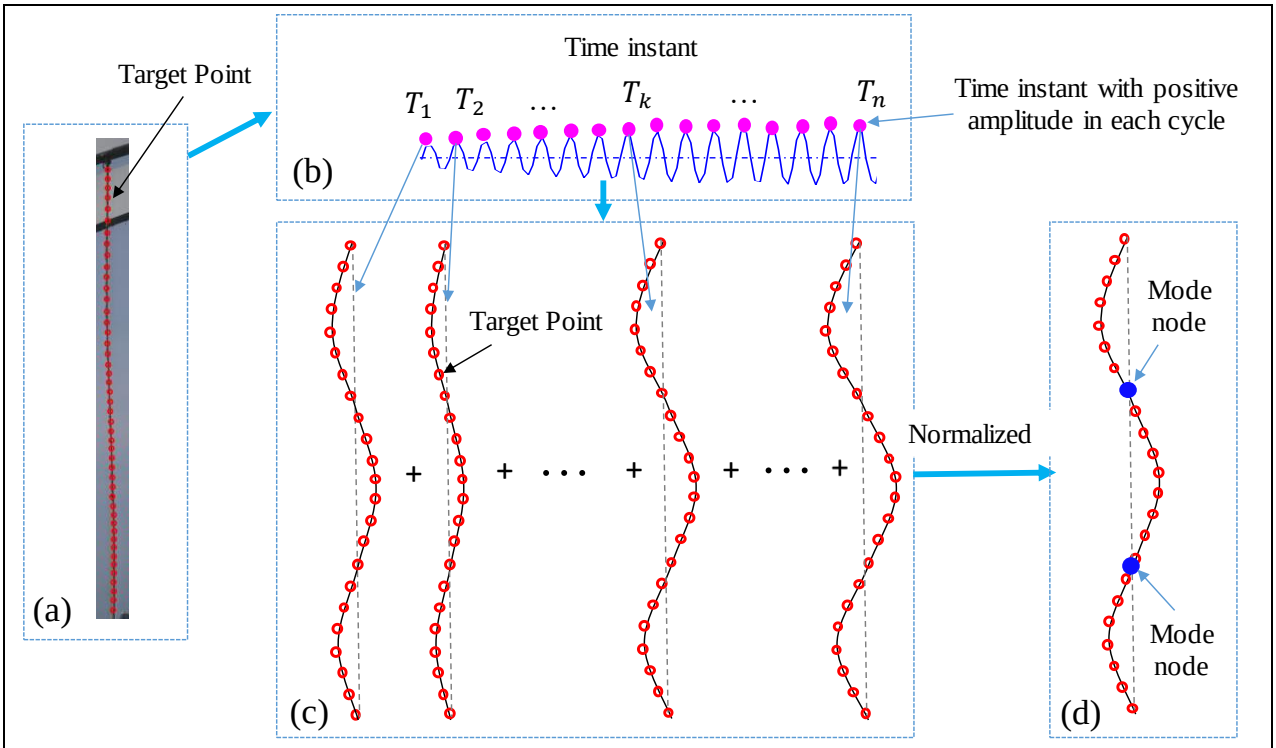

Fig.3. DIC-based operational deflection mode identification

2.4. *Cable force determination from measured mode shape*

As reported by Yan et al.,[6,7] the key to successful determination of the axial force of a cable with complex end conditions is to consider the segmental length of the modal nodes of the measured mode shape as the effective length of a pinned-pinned cable model. As shown in Fig. 1, for a cable with properties of length L, mass per unit length m, flexural rigidity EI, and cable force T, the intermediate segmental length L_{ij} between any two modal nodes i, j can be considered as the effective length of the cable with a natural frequency w_n. The equivalent intermediate segment model with L_{ij}, m, EI and $w_{ij} = w_n$ is then employed as a pinned-pinned cable model to estimate the tension force T and mathematically expressed as follows:

$$T = \frac{m w_n^2 L_{ij}^2}{(j-i)^2 \pi^2} - \frac{(j-i)^2 \pi^2 EI}{L_{ij}^2} \quad (1)$$

It is worth noting that the proposed approach may introduce inevitable estimation errors since

there is a difference between the segmental cable model with two pinned ends and the original cable model with complex end conditions. Yan et al.[6,7] conducted a relative error analysis to verify the validity of the proposed approach and their non-dimensional parametric studies yielding the following findings:

- The end constraints affect the segmental cable near the ends, and
- The proposed approach is feasible for long and slender cables, whereas for short cables, the mode order n and the other parameters such as supporting and rotation stiffness, the flexural rigidity of the cable, etc., should be carefully selected to achieve acceptable identification accuracy.

3. Laboratory Experimentation and Verification

3.1. *Experimental lab-test setup*

To verify the effectiveness of the proposed approach integrating PMM and DIC (PMM+DIC) for cable force determination, an experimentation test on a tensile inclined cable composed of a steel wire rope with a diameter of 4mm was conducted. As shown in Fig. 4, the cable has an inclined angle of 31°, a horizontal projection length of 2.4 m, and a vertical projection length of 2.4 m. One end of the cable is clamped to a steel beam anchored on the ground while the other end is connected to a weight (applying a tensile load to the cable) through a pulley system installed on a steel frame. Fifty-two steel blocks, each with a weight of 0.05 kg, were uniformly distributed and loaded along the cable at a spacing length of 50 cm.

The cable was slightly excited by a hammer near the bottom end to produce an artificial impulse force, however, the cable vibration may be invisible to the naked eye. The image sequence

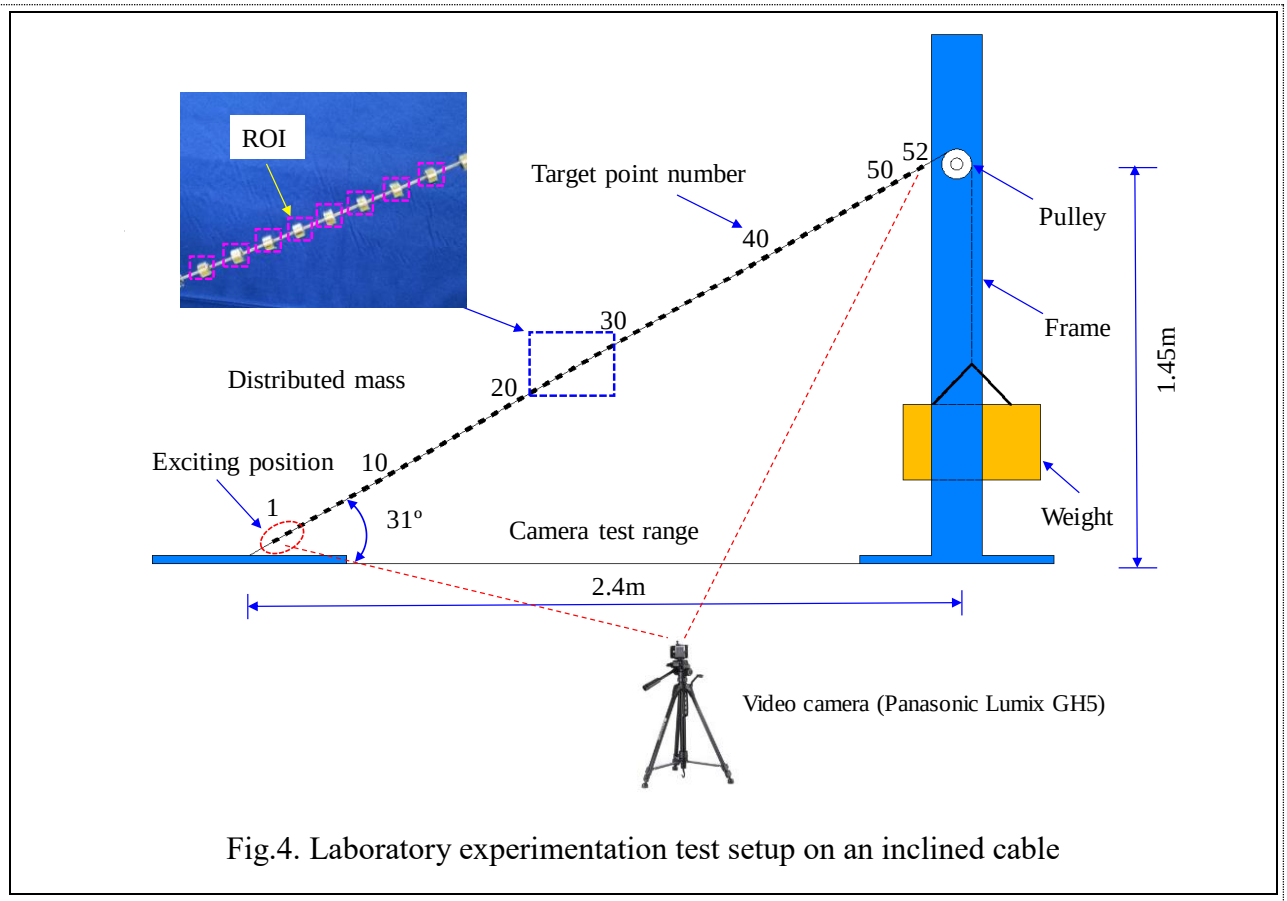

Fig.4. Laboratory experimentation test setup on an inclined cable

of the cable system was recorded using a consumer-grade video camera (Panasonic Lumix DC-GH5) equipped with a 14~42 mm lens. The camera is capable of recording video images from 50/60 frame per second (fps) at a resolution of 3840×2160 pixels (4K) to 180fps at a resolution of 1920×1080 pixels (1080P), respectively. Since the natural frequency of the fifth mode of the cable may approach 15 Hz, the experimental test setup employed a relatively higher resolution of 3840×2160 pixels (4K) at 60 fps to increase accuracy in capturing the image sequences of the cable.

3.2. *Laboratory test - implementation procedure*

An impact hammer near the bottom end of the cable was used to excite the cable every 25 to 30 seconds. Note that, as the cable is only weakly excited by the hammer, the cable vibration may not only be invisible to the naked eye but the DIC approach may also fail to track the target motion, resulting in unacceptable identification accuracy. Hence, some trial hammer-excitation tests were

conducted to ensure accurate implementation of the DIC through adjusting the amplitude of the excitation. The steel blocks along the cable were employed as the ROIs for the DIC-based target tracking by using the registration algorithms for FTCC and IC-GN in the integer pixel and sub-pixel levels, respectively. During this stage, the DIC was used to determine the resonance frequencies of the cable as a prior knowledge for the subsequent PMM procedural implementation.

Fig.5 shows plots of the typical displacement-time history and frequency spectrum of target No. 28, under slightly higher excitation for a total duration of 300s, when the cable force comprised of a weight equivalent of 320kN. It is observed that the first 5 modal frequencies (3.110, 6.321, 9.668, 12.876, and 15.645Hz) can be extracted via peak picking. The measured resonance frequencies are considered as the center frequencies f_c of the band-pass filters in the implementation of the PMM technique.

To ensure that the magnified motion is considered as the operational deflection shape of the cable as well as the center frequency of the band-pass filter, it is necessary to determine the critical parameters of the frequency bandwidth f_b and magnification factor α as the prior knowledge for implementing the PMM technique. Note that the tensile cable system generally has no closely-spaced modes, hence, it is easy to satisfy the requirement of the frequency bandwidth for mode separation when overlapping of the adjacent modes can be avoided. Moreover, for the magnification factor of the phases corresponding to the frequency band filtration process, the contribution of the vibration component of the mode to the overall displacement-time history of the cable is generally considered. For instance, when a high order mode of the cable contributes less to the vibration response, a higher magnification factor must correspondingly be adapted. However, too high an amplifier factor may undesirably produce distortion of the amplified motion images, resulting in

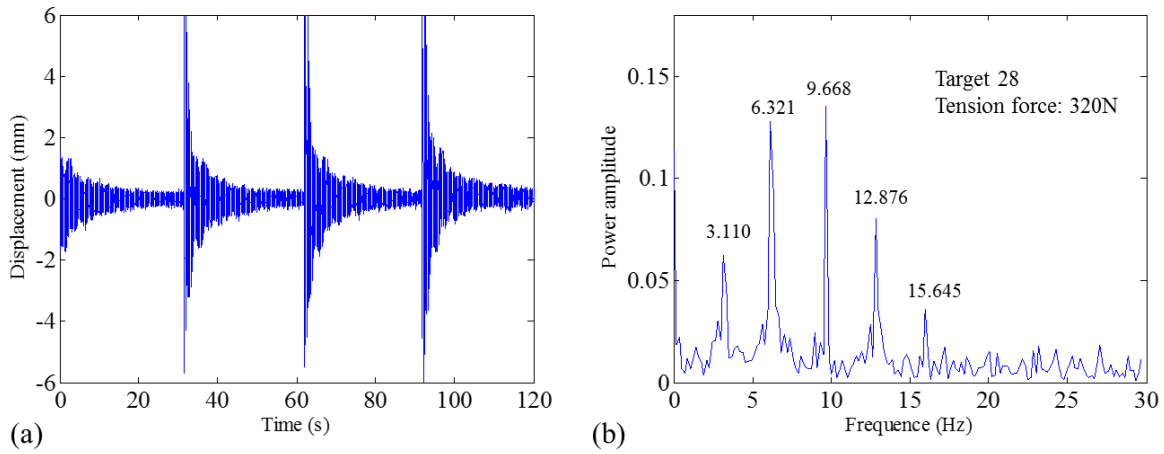

Fig.5. (a) Displacement-time history, and. (b) Frequency spectrum of target No.28.

the degradation of image quality for subsequent DIC-based displacement measurements.

To mitigate such scenarios as exemplified in the previous paragraph, trial tests were conducted to select a relatively higher (and optimum) amplifier factor α for satisfactory motion detection using the selected resonance frequencies. In this study, the frequency bandwidth f_b was set to be 1.0 Hz for all the resonance frequencies, and the amplifier factors α for the 2nd, 3rd, 4th, and 5th modes were set to 20, 50, 80, and 100, respectively. Due to the time-consuming nature of the PMM procedure, only 6.7s cable vibration video was considered in the laboratory experimentation test.

3.3. *Laboratory test results, analysis, and discussions*

Fig.6 (a-d) presents the snap shots of the motion-magnified cable related to the 2nd, 3rd, 4th, and 5th modes at the respective time instants corresponding to the frequencies shown in the figure. The DIC technique was used to extract the displacement-time history corresponding to the specific modes of interest through target tracking. It is observed in Fig. 6 that the estimated instant operational deflection shapes in the form of snap shots, showing acceptable image resolution of the cable motion, appear to be roughly in accordance with their corresponding modes. However, there appear to exist

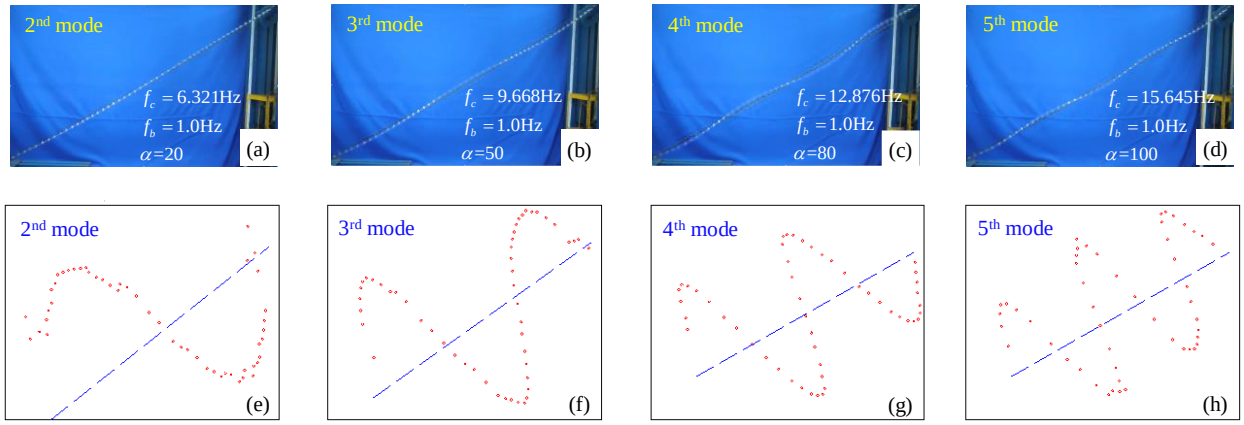

Fig.6. Snap shots of the motion magnified cable at specific time instants for: (a) 2nd mode, (b) 3rd mode, (c) 4th mode, and (d) 5th mode; and the addition of multi-groups of instant operational deflection shapes for: (e) 2nd mode, (f) 3rd mode, (g) 4th mode, and (h) 5th mode.

some slight distortions, shadows, and artifacts in the regions with relatively higher amplitude motions. For the implementation of DIC, the introduction of artifacts and other errant shadows in the image sequences of the magnified motion will likely degrade the quality of target tracking, and ultimately the final output results.

In this study, to avoid the deficiency of the traditional Canny edge detection method with respect to the motion-magnified video and maximum deflection, as shown in Fig. 3, *n* groups of instant operational deflection shapes estimated via DIC were added, normalized, and fitted to a Sine-type mode shape, which significantly improved the quality of the shapes. Fig.6 (e-h) shows the addition of multi-groups of instant operational deflection shapes to the discrete target points for the 2nd, 3rd, 4th, and 5th modes, respectively. It is seen that the discrete target points form an acceptable deflection mode shape.

Fig. 7(a-c) shows the Sine-type fitting for the operational deflection shapes of the discrete target points at (a) mode 3, (b) mode 4, and (c) mode 5, respectively. It is observed that the mode shapes fitted by the Sinusoidal functions[28] do not completely match with the discrete target points.

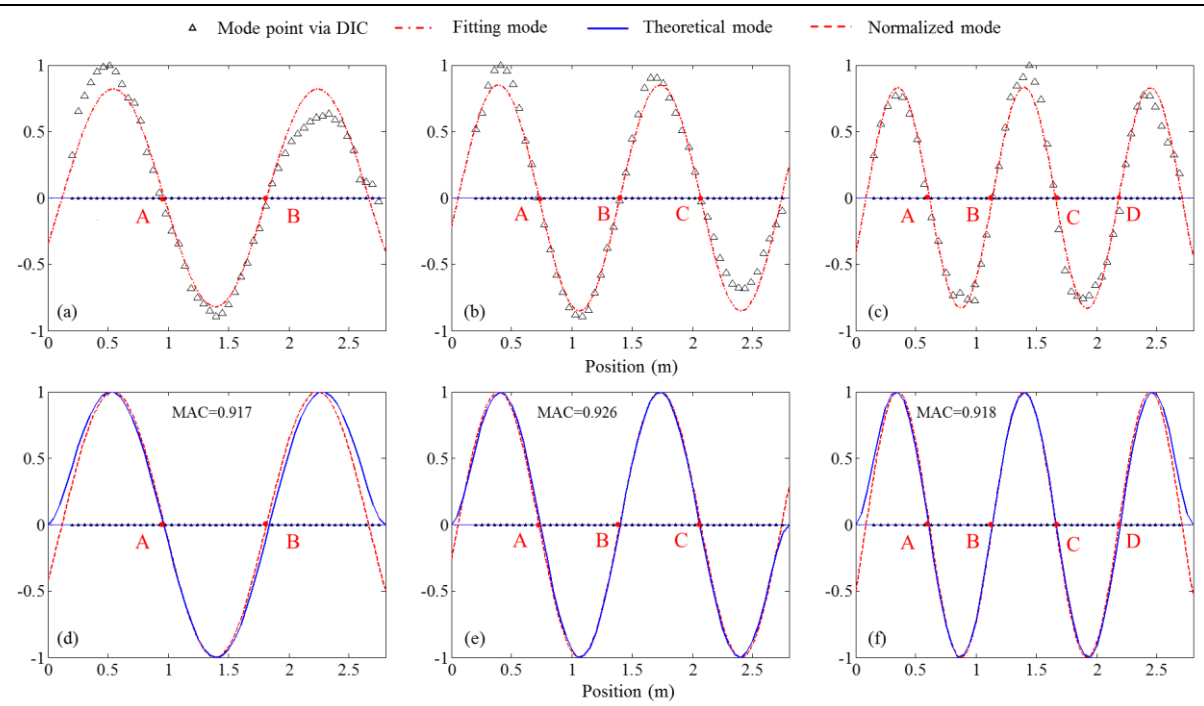

Fig.7. Fitting the operational deflection shapes of: (a) 3rd mode, (b) 4th mode, and (c) 5th mode; and, Comparisons of the normalized (experimental) shape with the theoretical shapes of: (d) 3rd mode, (e) 4th mode, and (f) 5th mode.

This is particularly pronounced for points with relatively higher motions, which may have been induced by the artifacts and shadows in the image sequences of the magnified motions, resulting in the target tracking error for the DIC registration algorithms. Fig. 7(d-f) shows graphical plots of the normalized experimental shape in comparison to the theoretical shapes. Apart from the start and end regions, the identified third, fourth, and fifth-order modes are very close to the theoretical modes. This indicates that the differences between the Sine-type fitted mode and the discrete target points appear to be not affect the identified modal nodes (zero-amplitude points). Furthermore, it is easy to visually locate the mode nodes in Fig. 6, e.g. nodes A, B, and C for the 4th mode.

For comparisons, Fig. 8 displays the comparative results of the experimental shapes estimated via combinations of the DIC and FDD (DIC+FDD) with the theoretical shapes. In the figure, the fitted mode shows good agreement with the theoretical mode, with curves nearly overlapping each

other.

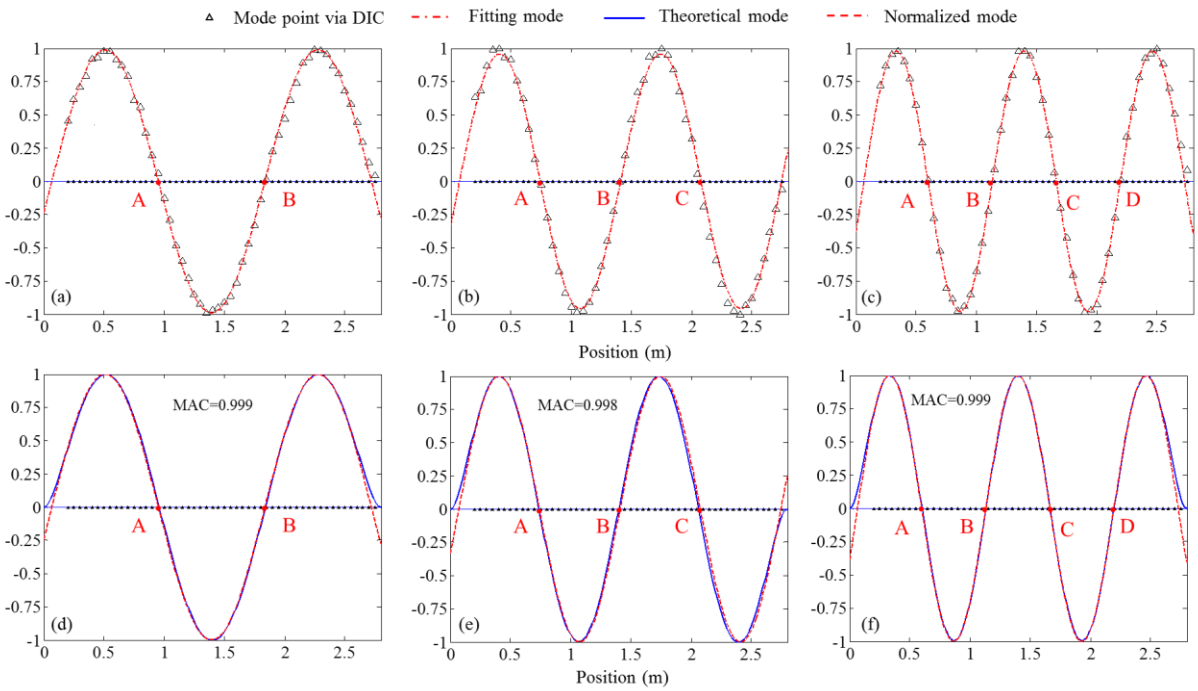

Fig.8. Fitting the operational deflection shapes of: (a) 3rd mode, (b) 4th mode, and (c) 5th mode; and, Comparisons of the normalized (experimental) shape with the theoretical shapes of: (d) 3rd mode, (e) 4th mode, and (f) 5th mode.

The distance of any two modal nodes can be easily extracted as the effective length of a tensile beam model with two hinged end conditions. The proposed approach significantly simplified the tension force estimation of the cable with complex boundary condition.

Table 1 shows a comparison of the estimated effective lengths and cable forces using the two methods, namely PMM+DIC and DIC+FDD. The modal assurance criterion (MAC) was employed to evaluate the similarity of the operational deflection shapes and theoretical mode shapes. Three observations are evident from Table 1 as follows:

Observation (1): both two methods are available to identify modes 3, 4, and 5 under weak excitation (PMM+DIC) or slightly higher excitation intensity (DIC+FDD). By contrast, the MAC values (0.917. 0.926, and 0.918) derived from PMM and DIC are much smaller than those derived

from the approach integrating DIC and FDD (0.999. 0.998, and 0.999). This can also be

Method	Excitation intensity	Mode order	Resonance frequency (Hz)	MAC	Mode nodes	Effective length（m）	Practical value（N）	Estimated value（N）	Relative error（%）
PMM + DIC	Weak	3	9.668	0.917	A-B	0.89	320	304.02	-4.99
		4	12.876	0.926	A-B	0.68	320	312.65	-2.29
					B-C	0.67	320	303.52	-5.15
					A-C	1.35	320	308.07	-3.73
		5	15.645	0.918	A-B	0.55	320	309.93	-3.15
					B-C	0.56	320	321.31	-0.41
					C-D	0.55	320	309.93	-3.15
					A-C	1.11	320	315.59	-1.38
					B-D	1.11	320	315.59	-1.38
					A-D	1.66	320	313.70	-1.97
DIC + FDD	Slightly higher	3	9.668	0.999	A-B	0.92	320	324.86	1.52
		4	12.876	0.998	A-B	0.69	320	321.91	0.60
					B-C	0.69	320	321.91	0.60
					A-C	1.38	320	321.91	0.60
		5	15.645	0.999	A-B	0.56	320	321.31	0.41
					B-C	0.57	320	332.88	4.03
					C-D	0.56	320	321.31	0.41
					A-C	1.13	320	327.07	2.21
					B-D	1.13	320	327.07	2.21
					A-D	1.69	320	325.14	1.61

Table 1. Comparisons of MAC and estimated cable forces.

observed from Fig. 7 and Fig. 8. As previously mentioned, slight distortions, shadows, and artifacts in the magnified motions via PMM degrade the quality of the DIC in target tracking. However, under the slightly higher excitation, the direct target tracking on the original video in the DIC procedure is not affected by distortions, shadows, and artifacts.

Observation (2): Although there are distinct differences between the MAC values in Table 1, the effective lengths between any two modal nodes can be extracted from the third, fourth, and fifth

operational deflection shapes. These results show some minor differences, which indicates that the positions of the modal nodes derived from the fitted shape are not significantly affected.

Observation (3): The two methods achieved acceptable identification accuracies with respect to practical cable force determination. This evidenced by the fact that the relative errors between the experimental values and the practical values in Table 1 are marginal, i.e., ranging from -5.15% to 4.03%, respectively.

4. Field Measurement and Validation

4.1. *Experimental field-test setup*

A field measurement on the hanger cable of an arch bridge was conducted to validate the proposed method. As shown in Fig. 9, the Fengguang bridge, located in Liuyang, Hunan Province (China), is a two-span half-through arch bridge with a length of 100 m for each span. The bridge deck is suspended from the arch ribs by 19 pairs of hanger cables, each with a spacing length of 4.0 m along the bridge longitudinal direction. One of the hanger cables near the span center was arbitrarily selected for the displacement measurement in this study.

As shown in Fig. 10, the calculation model for the hanger cable was established as a tensioned beam with two intermediate supports. The cable, with a total length of 20.682 m, is supported by two intermediate compressive-type high-damping rubber (HDR) dampers with a support stiffness of K_1=K_2 = 8.922×10^5 N/m. As can be seen in Fig. 10, the two damper supports divide the cable into three segments, with $x_1 = \varepsilon_1 L = 0.875\text{m}$ (which is the location of HDR damper at the deck-end) and $x_2 = \varepsilon_2 L = 1.282\text{m}$ (which is the HDR damper location of the arch rib-end), respectively. The mass per unit length of the cable is 12.107 kg/m, with an elastic modulus E and moment of inertia I of

365 1.95×10^{5} MPa and 1.62×10^{-7} m^4, respectively, for the cable.

Fig.9. Pictorial view of the Fengguang Bridge in Hunan Province, China

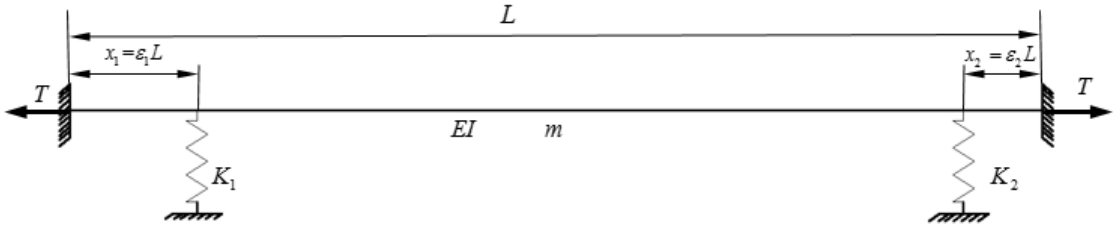

Fig.10. Hanger cable model.

366 **4.2.** ***Field measurement implementation procedure***

367 In the implementation of the modal shape identification process, the location of the target points
368 along the hanger cable should be predefined via an electric total station or machine vision-based
369 measurements. Numerous LED decorative lights, each with a spacing of 50 cm was attached along
370 the hanger cable, which can be regarded as the target points with distinct surface features in the DIC
371 procedure. Fig. 11 presents the experimental field-test setup for the DIC vision system. An
372 electronic total station (SOKKA CX-101) was used for the spatial positioning of the LED lights
373 along the cable. A video camera, Panasonic Lumix DC-GH5 equipped with a 100-400mm lens, was

set about 100m far from the hanger cable, with its pixel resolution configured to 3840×2160 pixels (4K)

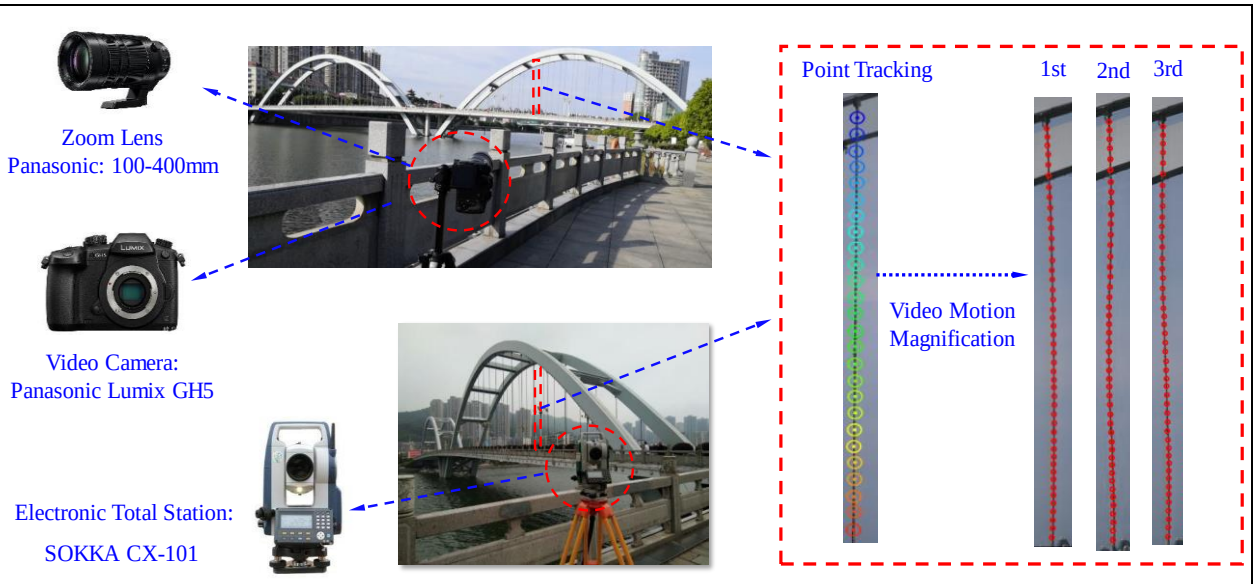

Fig.11. Field experimentation test setup on a bridge hanger cable

at a frame rate of 180 fps for displacement extraction. The focus lens was adjusted to adapt to the frame size covering the total selected hanger cable.

The Fengguang bridge is only accessible to buses and cars. Trial tests indicated that (other than traffic-induced excitation), environmentally induced vibrations, e.g., wind, etc., was difficult to excite the bridge hanger cable with significant vibration amplitudes that are adequate for vision-based displacement measurements and extraction via the DIC or PMM procedure. Consequently, manual hand shaking was applied to excite the hanger cable at the bridge deck-end with a time duration of about 6.7s with 400 frames for PMM and 60s for DIC processing. For comparison purposes, an accelerometer was installed on the cable at about 2.3 m from the bridge deck. The sampling frequency for the accelerometer was 100 Hz.

Like the laboratory test setup, the center frequencies for the PMM were also derived from the frequency spectrum via the DIC+FDD procedures. Fig. 12(a) shows the extracted multi-point

displacements of the target points on the hanger cable via the DIC procedure, where the red target point at the arch rib surface was regarded as a relatively stationary reference target with roughly

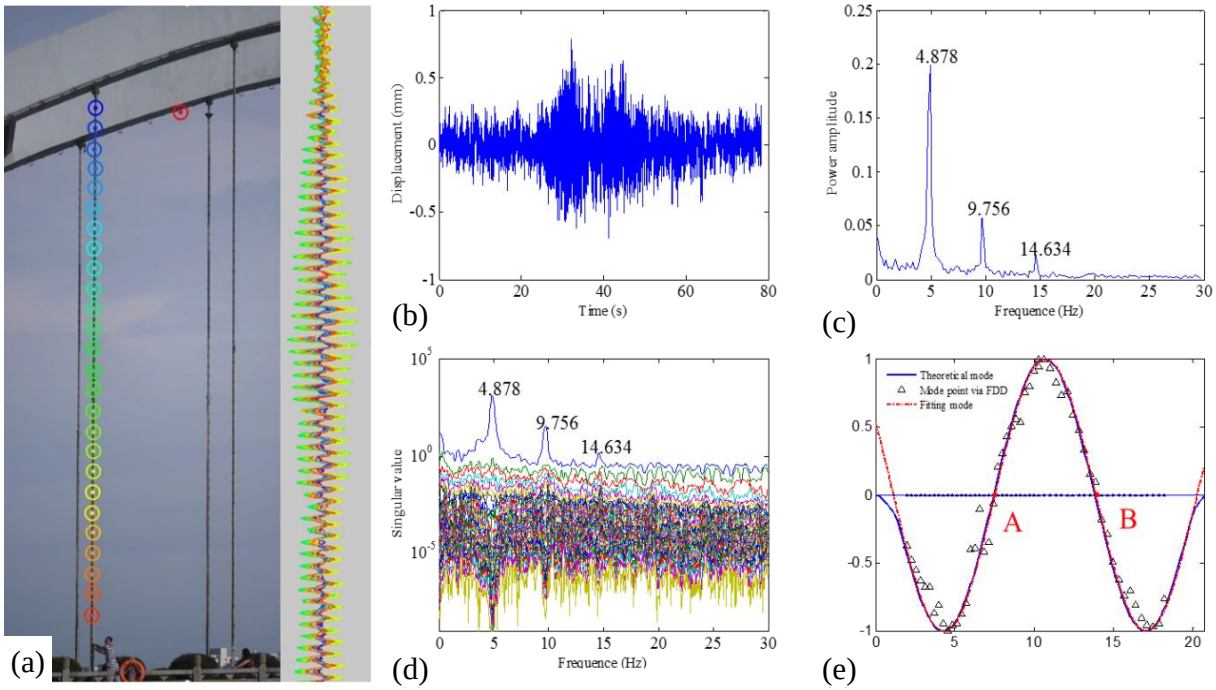

Fig.12. (a) Multi-point displacements of the hanger cable via DIC; (b) Displacement time history, and, (c) Power spectrum of a representative target point; (d) Singular values of power spectrum density matrix, and, (e) Third-order mode shape via FDD.

zero deflection. The displacement-time history and its power spectrum for a representative target point is plotted in Figs. 12(b) and (c), respectively. It is observed that the first three resonance frequencies (4.878, 9.756, and 14.634 Hz) are dominant within the frequency spectrum. These three frequencies were considered as the center frequencies or reference datum of the band-pass filters in the subsequent PMM procedural analysis. The singular values of power spectrum density matrix and the identified third-order mode shape via FDD are plotted in Figs. 12(d) and 12(e), respectively. It is seen that it is easy to visually locate the mode nodes A and B from the fitted third mode.

Table 2 lists the critical PMM parameters, in which the frequency bandwidths for the filters

were all set to 1.0 Hz. The amplification factors for modes 1, 2, and 3 were 20, 80, and 200, respectively. The quarter-octave CSP and FIR temporal filter were employed for phase amplification.

Modal order	Center frequency (Hz)	Frequency bandwidth (Hz)	Amplification factor	Decomposition in the frequency domain	Temporal filtering
1	4.878	1.0	20	Quarter Octave	FIR
2	9.756	1.0	80	Quarter Octave	FIR
3	14.634	1.0	200	Quarter Octave	FIR

Table 2. PMM parameters.

4.3. *Field test results, analysis, and discussions*

In this section of the paper, the comparative results of the three approaches, namely PMM+DIC, DIC+FDD, and accelerometer, respectively, for tension force determination of a hanger cable are presented. Fig. 13(b-d) shows screen-shots of the motion magnified hanger cable for the first three modes. Compared to the original video shown in Fig. 13(a), the motion-magnified operational deflection mode shapes corresponding to the dominant frequencies are distinctively visible to the naked eyes. It is interesting to note that, compared to the laboratory test, the typically existing distortions, shadows, and artifacts are not distinct in the motion-magnified snap-shot, particularly for the first two modes – which is the desired scenario. This may be attributed to the following factors: higher contrast between the surface characteristic feature and the background, stationary video camera system, and optimum parameters for the PMM procedural analysis.

For the third mode, its vibration component is relatively weak. A higher amplification factor of 200 was thus applied to the phase magnification. This high amplification may have collaterally magnified the effects of noise contamination, subsequently causing a deterioration of the mode shape as evident in Fig. 13 (d).

417 Fig. 14(a-c) shows the Sinusoidal functions fitted to the operational deflection shapes of the

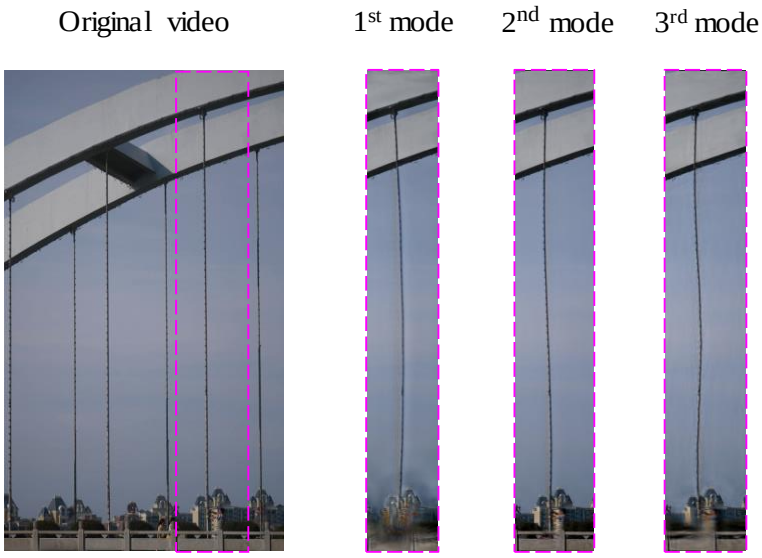

Fig.13. Screen snap shot of: (a) the original video, and, the motion magnified hanger cable at certain time instant for: (b) 1st mode, (c) 2nd mode, and, (d) 3rd mode.

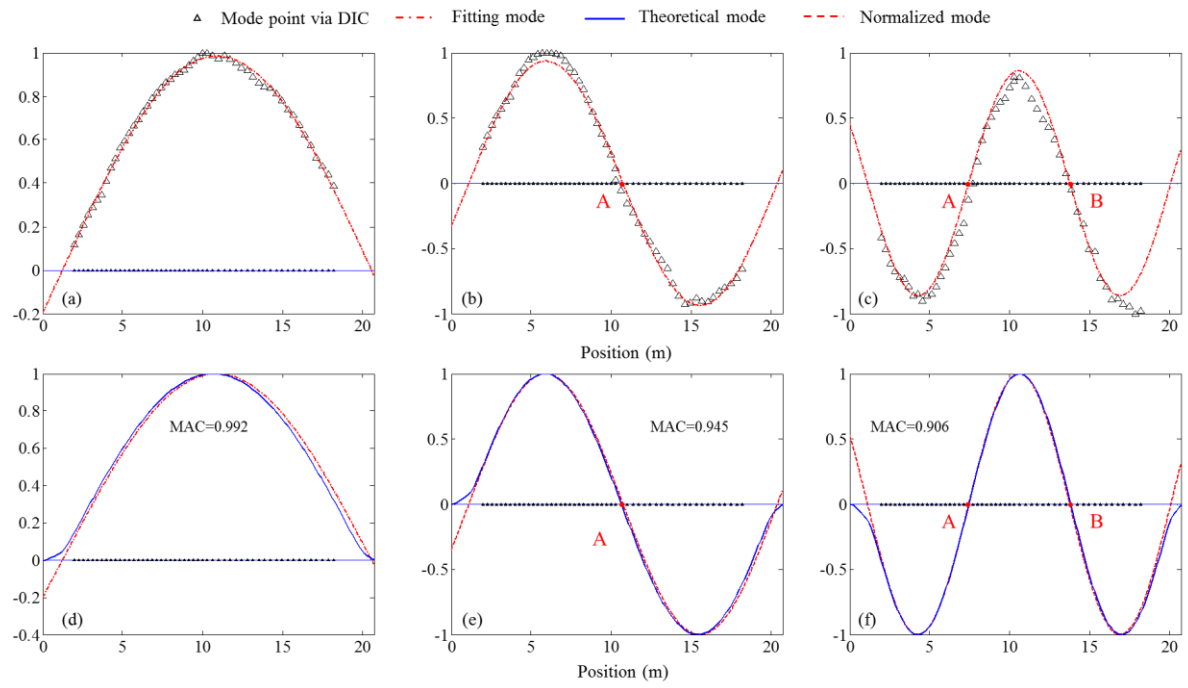

Fig.14. Fitting the operational deflection shapes of: (a) mode 1, (b) mode 2, and (c) mode 3; and, Comparisons of the normalized (experimental) shape with the theoretical shapes of: (d) mode 1, (e) mode 2, and (f) mode 3.

discrete target points at (a) mode 1, (b) mode 2, and (c) mode 3, respectively. It is observed that the mode points of the first two modes align well with the fitted Sine-type mode, whereas for the third mode, there are relatively higher variations in the mid-span regions that may have been induced by the tracking error of the DIC algorithms on the deteriorated target points. The MACs for modes 1, 2, and 3 are 0.992, 0.945, and 0.906, respectively, which partially proves the degradation of the third mode, i.e., the lowest MAC value.

Fig. 14(d-f) shows the difference between the theoretical and normalized fitting modes. Note that the theoretical mode shapes and the tension force were derived from the model shown in Fig.10 and the measured multiple-order resonance frequencies. Other than the obvious modal errors for the third-order mode (particularly at the start and end points), the errors appear to be having no significant effect on the accurate identification of the modal nodes after Sine-type wave fitting, e.g. nodes A and B for the third mode.

Compared with the identification results of DIC + FDD procedure, as shown in Figs. 12(d) and (e), the map of singular values of the power spectrum density matrix for the target displacements with respect to the frequency domain demonstrate that the three dominant frequencies can be clearly extracted. The vibration amplitude of the third mode appears to be the weakest one. Additionally, the adjacent frequency band around the third mode includes several small noise-induced frequency peaks, which may affect the identification accuracy of the third mode. Like the PMM results, the modal points align well with the fitted Sine-type operational deflection mode, especially for the target points with relatively higher amplitudes. However, the positions of the modal nodes appear to be consistent with the theoretical results. The MAC value for mode 3, as shown in Table 3, is

0.912, which partially proves the degradation of the third mode using DIC+FDD procedure.

Method	Mode order	MAC	Modal node	Effective length (m)	Exact force value (kN)	Estimated force value (kN)	Relative error (%)
PMM+DIC	3	0.906	A-B	6.31	410.6	405.1	-1.34
DIC+FDD	3	0.912	A-B	6.37	410.6	413.2	0.63
Accelerometer	1-5	-	-	-	410.6	410.6	0.0

Table 3. Comparisons of MAC values and estimated cable forces.

Table 3 shows a comparison of the estimated effective lengths and cable forces using the three methods, namely PMM+DIC, DIC+FDD, and accelerometer, respectively. It is seen that the identification results (i.e., effective lengths, force) of the PMM+DIC method do not differ significantly from the DIC+FDD method. For the third-order mode, the MAC values of the two methods are 0.906 and 0.912, respectively. According to the position of the two mode nodes of the fitted mode shape in the identification results (i.e., points A and B in Fig. 14), the effective lengths of the cable as determined by the two methods are 6.31m and 6.37m, respectively. Substituting these values (effective lengths) into Equation (1), the cable force was estimated as listed in Table 3, with the relative errors of the two methods being -1.34% and 0.63%, respectively.

It is worth noting that the exact values of the cable force listed in Table 3 (i.e., 410.6 kN) was calculated using the frequency-fitting method based on the natural frequencies of the cable measured by the accelerometer. The specific model used for these calculations was previously illustrated in Fig. 10.

5. Conclusions and Recommendations

A simple but effective non-contact target-free vision system integrating mode shape and a combination of the PMM and DIC methods was proposed for cable force determination. The identification accuracy of the integrated methodology was verified through laboratory testing on an inclined cable model and subsequently validated with field testing on hanger cables of a real

through-type arch bridge.

The laboratory verification test employed two approaches (PMM+DIC under weak excitation intensity and DIC+FDD under slightly higher excitation intensity) for mode identification. The laboratory test results indicated that slight distortions, shadows, and artifacts in the magnified motions using the PMM method degrade the quality of DIC sequence in target tracking. However, the positions of the modal nodes derived from the fitted shapes were not significantly affected. The relative errors between the experimental values and the practical values were within a range of -5.15% to 4.03%. Thus, the two methods satisfactorily achieved acceptable identification accuracies relative to practical cable force determination.

A field validation test on a typical hanger cable of a real-world through-type arch bridge demonstrated that the two modal nodes of the third-order modal shapes of the cable can be efficiently extracted using both PMM+DIC and DIC+FDD methods. Both methods can identify the 1st to 3rd modal shapes of the cable, with MAC values exceeding 90% (i.e., 0.90). The relative errors of the cable force were found to be -1.34% for the PMM+DIC approach and 0.63% for the DIC+FDD approach, respectively. Overall, the field validation test indicated that the proposed method has the potential to expediently estimate the tension forces of the cable with acceptable identification accuracy. The methodology exhibits practical viability and cost-effectiveness for routine application in cable tensile force determination.

Lastly, it is worth noting that the current study employed the third-order modal shape to extract the effective length of the cable from two mode nodes with zero amplitude. For stiff stayed cables or hanger cables, it is generally difficult to extract the third-order mode using the PMM or DIC-based vision system due to its weak vibrations in the cases of ambient (environmental) excitations

and even artificial shaking. Further research studies are thus recommended to explore the extraction of the cable effective length from the first or second-order modes using the proposed methodological system.

Acknowledgements and Disclaimer

The authors gratefully acknowledge the supports from the National Natural Science Fund of China (Grant Number: 51578227) and the fund of State Key Laboratory of Bridge Engineering Structural Dynamics and Key Laboratory of Bridge Earthquake Resistance Technology, Ministry of Communications, China. The authors acknowledge the assistance of Professor Zhu Mao, Department of Mechanical Engineering, University of Massachusetts Lowell for his help in the algorithms of video motion magnification.

The contents of this paper (which is not a standard nor specification) reflect the views of the authors who are solely responsible for the facts and accuracy of the data presented herein and do not necessarily reflect the official views or policies of any agency or institute. Trade names were used solely for information purposes and not for product endorsement, advertisement, promotions, or certification.

References

1. HM Irvine. Cable structures. The MIT Press, Cambridge, Massachusetts, and London, England. 1981.

2. EDS Caetano. Cable vibrations in cable-stayed bridges. IABSE-AIPC-IVBH, Zurich, Switherland. 2007.

3. H Zui, T Shinke, Y Namita. Practical formulas for estimation of cable tension by vibration method, *J. Struct. Eng.* **122**(6) (1996) 651-656.

4. WX Ren, G Chen. Practical formulas to determine cable tension by using cable fundamental frequency, *China Civil Engineering Journal.* **38**(11) (2005) 26-31.

5. Z Fang, JQ Wang. Practical formula for cable tension estimation by vibration method, *J Struct Eng.* **17** (2012) 161-164.

6. BF Yan, JY Yu, M Soliman. Estimation of cable tension force independent of complex boundary conditions, *J. Eng. Mech.* **141** (2014) 06014015.

7. BF Yan, WB Chen, JY Yu, XM Jiang. Mode shape-aided tension force estimation of cable with arbitrary boundary conditions, *J. Sound. Vib.* **440** (2019) 315-331

8. CC Chen, WH Wu, MR Leu, G Lai. Tension determination of stay cable or external tendon with complicated constraints using multiple vibration measurements, *Measurement.* **86** (2016) 182-195.

9. R Brincker, L Zhang, P Andersen. Modal identification of output only systems using frequency domain decomposition, *Smart. Mater. Struct.* (2001) 10:441

10. L Mevel, M Goursat, M Basseville. Stochastic subspace-based structural identification and damage detection and localization-application to the Z24 bridge benchmark, *Mech. Syst. and Signal Pr.* (2003) 1:143-151

11. B Pan. Digital image correlation for surface deformation measurement: Historical developments, recent advances and future goals. *Meas. Sci. Technol.* (2018) 29:082001.

12. B Pan. An evaluation of convergence criteria for digital image correlation using inverse compositional Gauss-Newton algorithm, *Strain.* **1**(50) (2014) 48-56.

13. YA Feng, FA Dai, H-HB Zhu. Evaluation of feature- and pixel-based methods for deflection measurements in temporary structure monitoring, *J. Civ. Struct. Health.* **5**(5) (2015) 615-628.

14. B Pan, L Tian, X Song. Real-time, non-contact and targetless measurement of vertical deflection of bridges using off-axis digital image correlation, *NDT & E Int.* (2016) 79:73–80

15. A Torralba, F Durand, C Liu, WT Freeman, EH Adelson. Motion magnification. *ACM T. Graphic.* **24**(3) (2005) 519-526.

16. N Wadhwa, M Rubinstein, F Durand, TF William. Phase-based video motion processing, *ACM. T. Graphic.* **32**(4) (2014) 80(1-10).

17. N Wadhwa, M Rubinstein, F Durand, WT Freeman. Riesz pyramids for fast phase-based video magnification, 2014 IEEE International Conference on Computational Photography (ICCP).

18. J Brieva, E Moya-Albor. Phase-based motion magnification video for monitoring of vital signals using the Hermite transform, 13th International Conference on Medical Information Processing and Analysis. Vol. 10572. International Society for Optics and Photonics.2017.

19. A Al-Naji, S-H Lee, J Chahl. An efficient motion magnification system for real-time applications, *Mach. Vision. Appl.* 29(4) (2018) 585-600.

20. BD Xue, SJ Zheng, WF Xue. Multi-scale adaptive factors video acceleration magnification, *Signal Processing: Image Communication.* 71 (2019) 36-44.

21. JG Chen, N Wadhwa, YJ Cha, F Durand, WT Freeman, O Buyukozturk. Modal identification of simple structures with h igh-speed video using motion magnification, *J. Sound. Vib.* 345 (2015) 58-71.

22. JG Chen, N Wadhwa, YJ Cha, F Durand, WT Freeman, O Buyukozturk. Developments with motion magnification for structural modal identification through camera video, *Dynamics of Civil Structures.* 2 (2015) 49-57.

23. YC Yang, C Dorn, T Mancini, Z Talken, G Kenyon, C Farrar, D Mascarenas. Blind identification

548 of full-field vibration modes from video measurements with phase-based video motion
549 magnification, *Mech. Syst. Signal. Pr.* 85 (2017) 567-590.
550 24. JG Chen, A Davis, N Wadhwa. Video camera-based vibration measurement for civil
551 infrastructure applications, *J. Infrastruct. Syst.* **23**(3) (2016) 11.
552 25. ZX Shang, ZG Shen. Multi-point vibration measurement and mode magnification of civil
553 structures using video-based motion processing, *Automat. Constr.* 93 (2018) 231-240.
554 26. A Sarrafi, P Poozesh, C Niezrecki, Z Mao. Detection of natural frequency and mode shape
555 correspondence using phase-based video magnification in large-scale structures, *Structural*
556 *Health Monitoring.* 6 (2019) 81-87.
557 27. AJ Molina-Viedma, L Felipe-Sese, E Lopez-Alba, FA Diaz. 3D mode shapes characterisation
558 using phase-based motion magnification in large structures using stereoscopic DIC, *Mech. Syst.*
559 *and Signal Pr.* 108 (2018) 140-155.
560 28. X Hu, F Zhou, S Hu, LF Walubita. Proposed loading waveforms and loading time equations for
561 mechanistic-empirical pavement design and analysis, *Journal of Transportation Engineering*.
562 **136**(6) (2010) 518-527.